Burrowing and subsurface locomotion in anguilliform fish: behavioral specializations and mechanical constraints

A. Herrel[1,2], H. F. Choi[3], E. Dumont[4], N. De Schepper[3], B. Vanhooydonck[2], P. Aerts[2] and D. Adriaens[3]

1. Département d'Ecologie et de Gestion de la Biodiversité, Muséum National d'Histoire Naturelle, 57 rue Cuvier, Case postale 55, 75231, Paris Cedex 5, France.

2. Department of Biology, University of Antwerp, Universiteitsplein 1, B-2610 Antwerpen, Belgium.

3. Department of Biology, Ghent University (U.G.), K.L. Ledeganckstraat 35, B-9000 Gent, Belgium.

4. Department of Biology, University of Massachusetts Amherst, 221 Morrill Science Center, 611 North Pleasant Street, Amherst, MA 01003, USA.

Short title: burrowing in anguilliform fish

pages: 18
tables: 1
figures: 5

Address for correspondence:
Anthony Herrel
Dépt. d'Ecologie et de Gestion de la Biodiversité
Muséum National d'Histoire Naturelle
57 rue Cuvier, CP 55   phone : ++33-140798120
75231, Paris   Fax : ++33-140793773
France   e-mail: anthony.herrel@mnhn.fr

Summary

Fish swimming is probably one of the most studied and best understood locomotor behaviors in vertebrates. However, many fish also actively exploit soil sediments. Because of their elongate body shape, anguilliform fishes are not only efficient swimmers but also very maneuverable. Consequently, many species live in complexly structured environments near the bottom and many are known to burrow into the sediment. To better understand burrowing and subsurface locomotion in anguilliform fish we provide descriptive kinematic data on subsurface locomotion in a burrowing eel (*Pisodonophis boro*) using videofluoroscopy. We also measure the maximal forces that can be exerted by this species during head-first and tail-first burrowing, and explore implications of head-first burrowing on mechanical stress distribution in the skull. Our data show that *P. boro* uses lateral undulation to penetrate and move in sandy soils under water. The kinematics of subsurface locomotion are different from those observed during swimming and are characterized by a very high slip factor. These observations differ considerably from recently published data in terrestrial sand-swimming lizards, and suggest that the sediment behaves like a solid rather than a frictional fluid. Finally, our finite element models show that the cranial shape and structure in the head-first burrowing *P. boro* is mechanically more suited for head-first burrowing in comparison to that of an obligate tail-first burrowing species, *Heteroconger hassi*.

Key words: locomotion, force, finite element model

Introduction

Fish swimming is probably one of the most studied and best understood locomotor behaviors in vertebrates (e.g. Lighthill, 1960, 1970; Videler and Wardle, 1991; Gillis, 1998; D'Août and Aerts, 1999; Sfakiotakis et al., 1999; Videler et al., 1999; Alexander, 2003). Different types of fish swimming are typically recognized depending on the involvement of the body during swimming, and range from anguilliform swimming where the whole body is used to provide propulsion, over ostraciform swimming where only the caudal fin moves and contributes to propulsion, to labriform swimming which is dependent on the use of the pectoral fins only (Sfakiotakis et al., 1999; Videler et al., 1999). However, many fish also exploit soil sediments (e.g. Tyler and Smith, 1992). Burrowing is an important behavior for many marine organisms; indeed, the faunal assemblages on muddy grounds in marine environments are dominated by burrowers (Atkinson and Pullin, 1996; Meysman et al., 2006). Because of their elongate body shape, anguilliform fishes are not only efficient swimmers (Van Ginneken et al., 2005) but also very maneuverable, and consequently many species live in complexly structured environments near the bottom of fresh and marine water bodies and are known to burrow into the sediment (Smith, 1989a,b; Nelson, 1994).

The mechanics of burrowing and sub-surface locomotion are generally not well understood as the mechanical properties of the substrate are often complex (Dorgan et al., 2007). Substrates such as sand can behave either as frictional fluids or granular solids depending on the stresses exerted on the substrate (Maladen et al., 2009; Mazouchova et al., 2010). Recent advances in mechanics of burrowing in small marine organisms (Dorgan et al., 2005, 2007; Che and Dorgan, 2010) and terrestrial sand swimming (Baumgartner et al., 2008; Maladen et al., 2009) have been made, but surprisingly little is known about burrowing or sub-surface locomotion in fish beyond the mouth-based excavation behavior observed in some species (Atkinson and Taylor, 1991; Atkinson and Pullin, 1996). Generally anguilliform fish use one of two modes of burrowing: tail-first and/or head-first soil penetration (De Schepper et al., 2007a,b). As burrowing in vertebrates is typically associated with the generation of large forces for penetrating the substrate (Ducey et al., 1993; O'Reilly et al., 1997), morphological or behavioral adaptations can be expected depending on whether organisms burrow head or tail first.

Fish are likely to adjust their behaviors depending on substrate mechanics, the speed of movement, the magnitude of forces exerted, and the type of sediment in which they are burrowing. For example in submerged granular soils one could expect the sediment to behave like a frictional fluid and fish could potentially use the same mechanism of locomotion (undulation) as is observed during swimming (cfr. sand swimming in lizards; see Baumgartner et al., 2008; Maladen et al., 2009). Alternatively, if the sediment behaves more like a solid, fish would likely switch to other modes of subsurface locomotion such as burrowing by compaction or crack propagation (see Gans 1973; Gans et al., 1978; Wake, 1993; Dorgan et al., 2005; Herrel and Measey, 2010). Depending on the type of behavior used, morphological and functional adaptations to soil penetration and sub-surface locomotion can be expected. For example, the tail of the obligate tail-first burrowing anguilliform fish, *Heteroconger hassi*, is characterized by a more rigid caudal fin (De Schepper et al., 2007a,b). Similarly, the skull of the facultative head-first burrower *Pisodonophis boro* shows reduced eyes, an elongate skull shape and strengthened cranial bones which are likely advantageous during head-first burrowing (Fig. 1; De Schepper et al., 2007a).

To better understand burrowing and subsurface locomotion in anguilliform fish we: 1) provide descriptive kinematic data on subsurface locomotion in a burrowing eel (*Pisodonophis boro*) using videofluoroscopy, 2) measure maximal forces that can be exerted by this species during head-first and tail-first burrowing, and 3) use finite element models (Dumont et al., 2005) to compare cranial form and structure in an obligate tail-first burrower (*Heteroconger hassi*; Congridae; Klausewitz and Eibl-Eibesfeldt, 1959) with a facultative head-first burrower (*Pisodonophis boro*, Ophichthidae; Hamilton, 1822). This allows us to explore whether cranial shape is indeed mechanically better designed for head-first substrate penetration as predicted (De Schepper et al., 2007a).

Materials and methods

Study animals

The fishes used in this study were obtained through the commercial trade, but are of unknown geographic origin. The *P. boro* eels were maintained at 25°C in a freshwater aquarium, the

bottom of which was covered with gravel. For the acquisition of the kinematic data, three individuals of *P. boro* were used. The *P. boro* individuals had a standard length of 17.0, 17.4 and 21.7 cm.

Videofluoroscopy

X-ray video recordings were made using a Redlake MotionPro (Redlake Inc., Talahassee, Fl) digital high-resolution camera attached to the image intensifier of a Philips Optimus M200 (Royal Philips Electronics, Amsterdam, The Netherlands) X-ray system. X-rays were generated at 40 kV and animals were filmed at 250 or 100 Hz while moving head- or tail-first through the sediment (Fig. 2A,B). Animals were filmed while moving horizontally in a 5cm layer of Rhine sand (max. particle size: 1mm) in a Perspex aquarium of 15 cm x 180 cm x 40 cm, and in which 10 cm of water was present. To help visualize movements of the animals small radio-opaque markers were inserted on the dorsal side of the animal under general anesthesia (MS222).

Kinematic analysis

Only sequences in which the eels were entirely in the field of view, were moving through the sand in a straight line, at constant speed, and which included at least one tail beat cycle were retained for analysis. Note, however, that as soon as part of the animal entered the field of view the steadiness of the locomotion speed could already be assessed. The swimming motions in the video sequences were analyzed throughout one cycle of the trailing edge (tail or snout tip, forward and backward swimming respectively). Each AVI-sequence was first down sampled to obtain about twenty frames per cycle that were subsequently saved as a JPEG-sequence. In each image the body midline was quantified by manually digitizing points on the midline of the fish using Didge (version 2.2.0, Alistair Cullum, Department of Biology, Creighton University, Omaha, NE). After digitization, the coordinates of these points were exported to Excel and raw data files were subsequently processed with custom routines written in MATLAB 6.0 (The Mathworks Inc., MA, USA).

The amplitude of the lateral body undulations was calculated for 11 equally spaced points along the body midline, the first and the last of which being the snout point and the tail tip, respectively. These points are further referred to as 'body points'. The positions of these body

points were calculated from the manually digitized coordinate sequences in the raw data files by means of a two dimensional cubic spline interpolation algorithm. The direction of motion was determined by performing a bi-variate linear regression (Sokal & Rohlf, 1998) on all the digitized midlines in a sequence. By applying a rotational coordinate transformation, the body midlines were rotated until the direction of motion coincided with the horizontal (X) axis so that the vertical (Y) coordinate of each body point equaled the distance of the lateral excursion of that point. The undulation amplitude in each body point was calculated as half the lateral distance covered between both extremes of the lateral excursions in a cycle. The wave period of the lateral undulations was determined as twice the time between needed for the posteriormost body point to reach its two most lateral positions. The undulation wave length was calculated as twice the mean distance between consecutive points on the body midline crossing the direction of motion, and the wave speed as the wave length divided by the wave period.

Overall locomotor speed was obtained by quantifying the path of the center of mass. Because the individuals had a fairly homogeneous body width, the mass was considered to be evenly distributed along the body. The position of the center of mass in each frame was therefore calculated by averaging the spatial coordinates of 51 equally spaced midline points. The distance covered by the center of mass was then plotted as a function of time and the average speed was calculated as the slope of the linear regression forced through the origin. The stride length was calculated as the swimming speed multiplied by the undulation period. The propeller efficiency (or slip factor), given as U/V (V = undulation wave speed, U = overall locomotor speed), was calculated as a measure of the propulsive efficiency.

Force measurements
Push forces were measured using a modified version of the set-up described in O'Reilly et al. (1997). Measurements of push forces during burrowing were made using a custom piezo-electric force platform (Kistler Squirrel force plate, ± 0.1 N; Kistler Inc. Winterthur, Switzerland). The force platform was positioned on a custom designed metal base and connected to a charge amplifier (Kistler Charge Amplifier type 9865). A Perspex block with 1cm deep holes of different diameters was mounted on the force plate level with the front edge (see Vanhooydonck et al., in press; Fig. 2C). One of the holes was loosely filled with wet sand from the aquarium of

the animal. A Perspex tunnel with a 90 degree angle in the horizontal plane and a diameter of about twice the maximal body diameter of the test animal was mounted on the metal base in front of (but not touching) the force plate and aligned with the soil-filled hole in the Perspex block. Next an animal was introduced into the tunnel (out of water) and allowed to move through it until reaching the soil-filled chamber. Next the animal was stimulated to burrow into the soil by tapping the end of the tail, or head respectively sticking out of the tunnel. Note that burrowing thus elicited is kinematically divergent from locomotion observed during voluntary sub-surface locomotion. The aim of this set-up was to elicit maximal forces from the animal rather than to mimic natural burrowing. Forces were recorded during a 60 second recording session at 1000Hz, and three trials were performed for each individual burrowing both head-first and tail-first. A recording session typically included multiple pushes of varying magnitude. As burrowing in *Pisodonophis* is characterized by undulatory movements in the horizontal plane, peak X and Y forces were extracted after low pass filtering (10Hz) using the Bioware software (Kistler). From all pushes recorded across all recording sessions only the highest forces were retained and used as external forces in our Finite Element models.

Histology and three dimensional reconstruction of the neurocranium
Specimens of both *P. boro*, a facultative head-first burrower and *Heteroconger hassi*, an obligate tail-first burrower, were commercially obtained and deposited in the Zoological Museum at Ghent University. The morphology of the head skeleton of both species was studied by serial cross sections. Specimens were fixed using a formaldehyde solution (8%), decalcified with Decalc 25% (HistoLab, Gothenburg, Sweeden), dehydrated through an alcohol series, and embedded in Technovit 7100 (Kulzer-Heraus, Hanau, Germany). Series of semi-thin sections (2 µm) were cut using a Leica Polycut SM 2500 (Wetzlar, Germany), stained with toluidine blue and mounted with DPX. Images of the sections were obtained using a digital camera (Colorview 8, Soft Imaging System, Olympus, Japan) mounted on a light microscope (Polyvar-Reichert) and processed with Analysis Docu (Soft Imaging System, version 3.0, Olympus, Japan). On the basis of the serial histological sections graphical 3D reconstructions were generated using Corel-Draw 8 (Corel) for tracing of the contours of the structures, and Amira 3.0 (TGS) and Rhinoceros 3.0 (McNeel) for making 3-D reconstructions of the neurocranium. For a detailed description of this cranial morphology, we refer to De Schepper *et al.* (2007a).

Finite element modeling

Methods for generating a 3D FE model from the 3-D reconstructed neurocrania follow Dumont, et al. (2005). We used Geomagic Studio (Raindrop Geomagic Inc.) to smooth the surface model based on the 3-D reconstructions of the neurocranium derived from histological sections. Surface models were saved from Geomagic as STL files and then imported to the FE analysis tool Strand7 (Strand7 Pty Ltd.). We used the solid mesh generation algorithm in Strand7 to create a volumetric mesh composed of four-noded tetrahedrals from each surface model. As models were different in size, we scaled loads derived from our *in vivo* measurements of burrowing forces in *P. boro* to the total model surface area in both species (*P. boro* and *H. hassi*) for comparative purposes (Dumont et al., 2009). We applied kinematic constraints to the models at four points along the edge of the foramen magnum, the point of contact between the neurocranium and the vertebral column). Maximal measured forces obtained from force plate recordings of *P. boro* were distributed homogeneously across the lateral and frontal side of the neurocranium in two different simulations referred to as the 'lateral' and 'dorsal' loading condition. The resulting FE output was analyzed by inspecting contour plots and the quantitative output of the results to compare and contrast the distribution and magnitude of von Mises stress, a predictor of ductile failure in cortical bone due to distortion or shear (Nalla et al., 2003).

We assigned the models mean values for the material properties of vertebrate bone (E = 20 GPa; Poisson ratio = 0.3; see Erickson et al., 2002). We modeled bone as homogeneous and isotropic. Even though this is not likely to be the case (Currey, 2002), applying orthotropic material properties appears to have little effect on global patterns of strain (or stress) in geometrically complex structures such as skulls (Strait et al., 2005). Because we applied the same material properties to both of our models and controlled for the effects of size, we can confidently compare stress distributions between them and attribute the differences observed to differences in neurocranial shape. However, the absolute values of stress predicted by our model may not reflect actual values and should be interpreted with caution.

Statistical analyses

Kinematic data were Log_{10} transformed prior to analyses. First, we used Pearson correlations to explore the effects of overall locomotor speed on kinematic variables. As speed effects were

significant for several variables we used a MANCOVA with total fish length and locomotor speed as co-variates to test for differences in locomotor kinematics between head-first and tail-first sub-surface locomotion.

Results

Kinematics of burrowing

Pisodonophis boro moved through the substrate (sand) using lateral undulation movements, both when moving head-first and tail-first (Table 1; Fig. 2). Correlations between overall locomotor speed and wave frequency and locomotor speed and wave speed were significant for both head-first (wave frequency~locomotor speed: $r = 0.93$, $P = 0.02$; wave speed~locomotor speed: $r = 0.98$; $P = 0.003$) and tail-first burrowing (wave frequency~locomotor speed: $r = 0.96$, $P < 0.001$; wave speed~locomotor speed: $r = 0.98$; $P < 0.001$). None of the other kinematic variables were correlated with overall locomotor speed (Fig. 3). A MANCOVA testing for differences between head-first and tail-first locomotion indicated no significant differences in kinematics between the two behaviors (Wilks' Lambda = 0.57; $F_{5,5} = 0.75$ $P = 0.62$). Effects of total length (Wilks' Lambda = 0.12; $F_{5,5} = 7.54$ $P = 0.02$) and locomotor speed (Wilks' Lambda = 0.00; $F_{5,5} > 1000$; $P < 0.01$) were, however, highly significant.

Force measurements

Upon introduction into the plexiglass tunnel, animals eagerly pushed either their heads or tails into the wet sand provided in the hole of the plexiglass block mounted on the force plate. Forces were highest in the X-direction during both head-first (0.99 ± 0.4N average $\pm$ STD; $N = 3$) and tail-first (2.45 ± 1.32N) pushes suggesting a largely uni-directional penetration of the substrate (Fig. 4). Whereas the maximal peak forces in the X-direction across all individuals were larger during tail-first soil penetration, peak forces in the Y-direction were larger during head-first (0.51 ± 0.25N) compared to tail-first (0.16 ± 0.05N) pushes. Peak forces in the vertical (Z) direction were variable and ranged from 0.58 ± 0.44N for head-first to 0.35 ± 0.09N for tail-first pushing.

Finite element modeling

Our finite element analyses indicate differences in both the distribution and magnitude of stress in the models of the two species. The elevated stresses around the foramen magnum in both

models are caused by the kinematic constraints in that region (Fig. 5); they do not affect stress in other portions of the skull and were ignored further. In general, stress magnitudes were higher in the *H. hassi* model compared to the *P. boro* model in the dorsal loading scenario when scaled to similar loading conditions (i.e. equal force to surface area; peak Von Mises: 48.82 and 24.34 in *H. hassi* and *P. boro* respectively). Peak stresses were similar, however, in the lateral loading condition (peak Von Mises: 34.88 and 34.46 in *H. hassi* and *P. boro* respectively). Regions of high stress were limited to the inter-orbital septum and the trabecula in *H. hassi* with a homogeneous and low stress distribution on the neurocranium (Fig. 5). This results in a steep stress gradient at the caudal aspect of the inter-orbital septum and the trabecula. In *P. boro*, however, stress concentrations in the inter-orbital septum and trabecula were less marked but stress in the brain case was more prominent, resulting in a shallower stress gradient at the caudal side of the inter-orbital septum (Fig. 5).

Discussion

Kinematics of subsurface locomotion

Our videofluoroscopic and observational data both suggest that *P. boro* uses lateral undulation to move in the sediment in our experimental set-up. Moreover, our observations of fish in the lab and studies quantifying tunnel shape in obligate tail-first burrowers, such as *H. hassi* and *H. longissimus* suggest that these species also use undulatory movements during burrowing (Tyler and Smith, 1992). Interestingly, head-first burrowing in *P. boro* was kinematically identical to tail-first burrowing and consisted of undulatory movements. This observation corresponds to the similar pattern observed during forward and backward swimming in this species (Herrel *et al.*, in press).

However, despite the overall similarity of the movements of *P. boro* during swimming and burrowing, there are significant quantitative differences between locomotion in the two media. During both head-first and tail-first burrowing, the amplitude of the tail-tip is greater than the average undulation amplitude, suggesting amplified tail movements compared to the movements of the rest of the body. Moreover, the slip factor during burrowing is significantly higher (around 1 on average) compared to swimming (0.5 on average) indicating that the wave of undulation travels down the body at the same speed as the animal's forward velocity. This implies that the

10

sediment behaves more like a solid and that little or no energy is lost due to movements of the sediment. Finally, the wave length is significantly greater during swimming compared to burrowing while the stride length remains identical (compare Table 1 to Table 1 in Herrel et al., in press). This indicates the presence of more undulatory waves across the body during burrowing. It can be hypothesized that the more wave fronts traveling at any given time along the body, the more distributed the propulsive forces over the body surface will be, and hence the lower the peak forces on any given body segment. Presumably, this allows for the observed minimal slip and the efficient propulsion. However, these observations need to be verified experimentally using empirical measurements of drag forces in water saturated granular sediments (see Maladen et al., 2009).

Interestingly, whereas *P. boro* used lateral undulations to move through the sediment, many terrestrial elongate and limbless animals use different ways of burrowing. For example, radically divergent mechanisms, including hydrostatic locomotion in caecilians or freight-train burrowing in uropeltid snakes, are used to penetrate and move through the sediment and allow them to generate considerably higher forces than would be possible using lateral undulation mechanics (Gans, 1973; Gans et al., 1978; O'Reilly et al., 1997). The use of lateral undulation for substrate penetration and sub-surface locomotion may be unique to granular media like sand as these media can behave like frictional fluids. In contrast, on land many elongate animals including eels and snakes typically use surface irregularities to push against and provide static points of friction called push points. However, the subsurface locomotion observed in *P. boro* appears to be different from that observed as indicated by the slip factor being close to one. Even though this resembles terrestrial lateral undulation in some ways, at the same time it differs in the absence of specific push points (Gans, 1974; Edwards, 1985). A slip factor of nearly one is about twice as high as has been observed for sandfish lizards (Maladen et al., 2009) and much higher than observed during swimming in eels and other fish (Videler et al., 1999). Essentially this implies that the substrate behaves like a solid with no displacement of sediment particles. Yet, *P. boro* is able to move through such media with ease indicating that the mechanics of sub-surface locomotion in water saturated granular media may be radically different and need to be investigated further.

11

Is head shape tuned to demands for burrowing?

The results from our finite element modeling suggest that the skull shape in the facultative head-first burrower *P. boro* may indeed be mechanically more suited to withstand stresses generated by head-first burrowing, compared to the obligate tail-first burrower *H. hassi*. Given the species-specific geometry and identical loading regimes, peak stresses were lower in *P. boro* compared to *H. hassi*. Moreover, loading the skull caused a strong stress concentration in the inter-orbital septum and the trabecula in *H. hassi,* resulting in pronounced stress gradients. The overall shape of the skull in *P. boro*, combined with the thicker bones (Tilak and Kanji, 1969; De Schepper et al., 2007a), may allow it to lower stress concentrations and to avoid high stress gradients. Additionally, the high degree of curvature in the interorbital septum in *H. hassi* likely results in both tensile and compressive stress. In contrast, in *P. boro* the interorbital septum is aligned with the long axis of the head causing compressive stresses on the bone only during frontal loading (as observed during our force measurements). Posterior to the interorbital septum, the frontal bones in the cranial vault are fused (De Schepper et al., 2007a). Given that bone is stronger in compression than tension (Currey, 2002), these data suggest that the skull in *P. boro* is indeed mechanically better suited for head-first burrowing than is the skull of *H. hassi*. Also the overall head shape, being rather pointed in *P. boro*, suggests it is better adapted for frontal soil penetration. More extensive modifications in the skull that have been linked to burrowing are, however, observed in other anguilliform species, such as moringuid eels (De Schepper et al, 2005). The observed higher forward pushing forces generated by the tail in *P. boro*, compared to the head, supports the hypothesis that this species may perform best at tail-first burrowing as was suggested based on morphological data (De Schepper et al., 2007a). Analyses of burrowing in a broader comparative sample of anguilliform fish with different head and tail shapes are, however, essential to test whether the differences in skull and tail shape are truly adaptive.

Acknowledgements

References

Alexander, R. McN. (2003). *Principles of Animal Locomotion*. Princeton & Oxford: Princeton University Press.

Atkinson , R. J. A. and Taylor, A. C. (1991). Burrows and burrowing behavior in fish. In: P.S. Meadows and A. Meadows (eds.) The environmental impact of burrowing animals and animal burrows. *Symp. Zool. Soc. Lond.* **63**, 133-155.

Atkinson, R. J. A. and Pullin, R. S. V. (1996). Observations on the burrows and burrowing behavior of the red band fish, *Cepola rubescens* L. *Marine Ecol.* **17**, 23-40.

Baumgartner, W., Fidler, F., Weth, A., Habbecke, M., Jakob, P., Butenweg, C. and Böhme, W. (2008). Investigating the locomotion of the sandfish in desert sand using NMR-imaging. *PLoS ONE* **3**, e3309.

Che, J. and Dorgan, K. M. (2010). It's tough to be small: dependence of burrowing kinematics on body size. *J. Exp. Biol.* **213**, 1241-1250.

Currey, J. D. (2002). *Bones: structure and mechanics.* Princeton: Princeton University Press.

D'Août, K. and Aerts, P. (1999). A kinematic comparison of forward and backward swimming in the eel *Anguilla anguilla*. *J. Exp. Biol.* **202**, 1511-1521.

De Schepper N., Adriaens D. and De Kegel B. (2005). *Moringua edwardsi* (Moringuidae : Anguilliformes): Cranial specialization for head-first burrowing? *J. Morphol.* **266,** 356-368.

De Schepper, N., De Kegel, B. and Adriaens, D. (2007a). *Pisodonophis boro* (Ophichthidae: Anguilliformes): specialization for head-first and tail-first burrowing? *J. Morphol.*, **268**, 112-126.

De Schepper, N., De Kegel, B. and Adriaens, D. (2007b). Morphological specializations in heterocongrinae (Anguilliformes: Congridae) related to burrowing and feeding. *J. Morphol.* **268**, 343-356.

Dorgan, K. M., Jumars, P. A., Johnson, B. D., Boudreau, B. P. and Landis, E. (2005). Burrow elongation by crack propagation. *Nature* **433**, 475.

Dorgan, K. M., Awade, S. R. and Jumars, P. A. (2007). Burrowing in marine muds by crack propagation: kinematics and forces. *J. Exp. Biol.* **210**, 4198-4212.

Ducey, P. K., Formanowicz, D. R., Boyet, L., Mailloux, J., Nussbaum, R. A. (1993). Experimental examination of burrowing behavior in caecilians (Amphibia, Gymnophiona) - effects of soil compaction on burrowing ability of four species. *Herpetologica* **49**, 450-457.

Dumont, E. R., Piccirillo, J. and Grosse, I. R. (2005). Finite element analysis of biting behavior and bone stress in the facial skeletons of bats. *Anat. Rec.* **293**, 319-330.

Dumont, E. R., Grosse, I. R. and Slater, G. J. (2009). Requirements for comparing the performance of finite element models of biological structures. *J. Theor. Biol.* **256**, 96-103.

Edwards, J. L. (1985). Terrestrial locomotion without appendages. In *Functional vertebrate morphology* (ed. M. Hildebrand, D. M. Bramble, K. F. Liem and D. B. Wake), pp.159-172. Cambridge: Harvard University Press.

Erickson, G. M., Catanese, J. III. and Keaveny, T. M. (2002). Evolution of the biomechanical material propertiesof the femur. *Anat. Rec.* **268**, 115-124.

Gans, C. (1973). Locomotion and burrowing in limbless vertebrates. *Nature* **242**, 414-415.

Gans, C. (1974). *Biomechanics: an approach to vertebrate biology*. Philadelphia: Lippincot.

Gans, C., Dessaur, H. C. and Baic, D. (1978). Axial differences in musculature of uropeltid snakes: the freight-train approach to burrowing. *Science* **199**, 189-192.

Gillis, G. B. (1998). Environmental effects on undulatory locomotion in the American eel *Anguilla rostrata*: kinematics in water and on land. *J. Exp. Biol.* **201**, 949-961.

Herrel, A., Choi, H.-F., De Schepper, N., Aerts, P. and Adriaens, D. (in press) Kinematics of swimming in two burrowing anguilliform fishes. *Zoology*

Herrel, A. and Measey, G. J. (2010) The kinematics of locomotion in caecilians: effects of substrate and body shape. *J. Exp. Zool.* **313A**, 301-309.

Lighthill, M. J. (1960). Note on the swimming of slender fish. *J. Fluid Mech.* **9**, 305-317.

Lighthill, M. J. (1970). Aquatic animal propulsion of high hydromechanical efficiency. *J. of Fluid Mech.* **44**, 265-301.

Maladen, R. D., Ding, Y., Li, C. and Goldman, D. I. (2009). Undulatory swimming in sand: subsurface locomotion of the sandfish lizard. *Science* **325**, 314-318.

Mazouchova, N., Gravish, N., Savu, A. and Goldman, D. I. (2010) Utilization of granular solidification during terrestrial locomotion of hatchling sea turtles. *Biol. Lett.* 6: 398-401.

Meysman, F. J. R., Middelburg, J. J. and Heip, C. H. R. (2006). Bioturbation: a fresh look at Darwin's last idea. *Trends Ecol. Evol.* **21**, 688-695.

Nalla, R.K., Kinney, J. H., and Ritchie, R. O. (2003). Mechanistic failure criteria for the failure of human cortical bone. *Nat Mater* **2**, 164–168.

Nelson, J. S. (1994). *Fishes of the World* (third edition). New York: Wiley & Sons.

O'Reilly, J. C., Ritter, D. A., and Carrier, D. R. (1997). Hydrostatic locomotion in a limbless tetrapod. *Nature* **386**, 269-272.

Sfakiotakis, M., Lane, D. M. and Davis, J. B. C. (1999). Review of fish swimming modes for aquatic locomotion. *IEEE Journal of Oceanic Engineering* **24**, 237-252.

Smith, D. G. (1989a). Family Anguillidae. In *Fishes of the Western North Atlantic. Part 9, vol. 1. Orders Anguilliformes and Saccopharyngiformes* (ed. B. Böhlke), pp. 25-47. New Haven: Yale University Press.

Smith, D. G. (1989b). Family Congridae. *Fishes of the Western North Atlantic. Part 9, vol. 1. Orders Anguilliformes and Saccopharyngiformes* (ed. B. Böhlke), pp. 460-567. New Haven: Yale University Press.

Sokal, R. R. and Rohlf, F. J. (1998). *Biometry* (third edition). New York: W. H. Freeman & Company.

Strait, D. S., Wang, Q., Dechow, P. C., Ross, C. F., Richmond, B. G., Spencer, M. and Patel, B. A. (2005). Modeling elastic properties in finite element analysis: How much precision is needed to produce an accurate model? *Anat. Rec.* **283A**, 275-287.

Tilak, R. and Kanji, S. K. (1968). Studies on the osteology of *Pisodonophis boro* (Hamilton). *Gegenbaurs Morphol. Jahrb.* **113-4**, 501-523.

Tyler, J. C. and Smith, C. L. (1992). Systematic significance of the burrow form of seven species of Garden eels (Congridae: Heterocongrinae). *American Mus. Novitates* **3037**, 1-13.

van Ginneken, V., Antonissen, E., Müller, U. K., Booms, R., Eding, E., Verreth, J. and van den Thillart, G. (2005). Eel migration to the Sargasso: remarkably high swimming efficiency and low energy costs. *J. Exp. Biol.* **208**, 1329-1335.

Vanhooydonck, B., Boistel, R., Fernandez, V. and Herrel, A. (in press). Push and bite: trade-offs between burrowing and biting in a burrowing skink (*Acontias percivali*). *Biol. J. Linn. Soc.*

Videler, J. J. and Wardle, C. S. (1991). Fish swimming stride by stride: speed limits and endurance. *Rev. Fish. Biol. Fish.* **1**, 23-40.

Videler, J. J., Muller, U. and Stamhuis, E. J. (1999). Aquatic vertebrate locomotion: wakes from body waves. *J. Exp. Biol.* **202**, 3423-3430.

Wake M. H. (1993). The skull as a locomotor organ. In *The Skull*, vol. 3 (ed. J. Hanken and B. K. Hall), pp. 197-240. Chicago: University of Chicago Press.

Figure legends

Figure 1: images illustrating the difference in cranial morphology and the shape of the neurocranium of two burrowing eels; A) *Heteroconger hassi*, an obligate tail-first burrower and B) *Pisodonophis boro*, a facultative head-first burrower. Note the difference in the shape of the head and endocranium being much more pointed and robust in *P. boro*. Endocranial images are derived from 3-D reconstructions based on histological sections.

Figure 2: images extracted from the X-ray video recordings of *P. boro* burrowing in sand. In A) the animal moves head-first; in B) tail-first through the substrate. The arrow represents the direction of movement which is from left to right in both cases. Note the typical undulatory movements used, similar to those observed in the same species while swimming. In A the sand was seeded with radio-opaque markers in an attempt to visualize soil displacement during burrowing. C) Schematic illustration of the set-up used to measure peak burrowing forces. The animal is introduced into the tunnel mounted on a metal base level with, but not touching the force plate. Next the animal pushes into the soil-filled chamber and the forces in X-, Y- and Z-directions are recorded.

Figure 3: graphs illustrating the effect of locomotor speed on the kinematics of undulatory burrowing. Closed symbols represent head-first, open symbols represent tail-first locomotion cycles. Whereas for both head-first and tail-first sub-surface locomotion an increase in overall

locomotor speed is associated with an increase in wave frequency (A), no correlation is observed between locomotor speed and the amplitude of the waves at mid-body (B).

Figure 4: representative force profiles for head-first and tail-first burrowing in *P. boro*. Note that movements are largely restricted to the horizontal plane with the animal pushing its head or tail straight into the substrate resulting in large forces in the X-direction.

Figure 5: results of the finite element analysis of models of *H. hassi* (left) and *P. boro* (right) under two loading conditions (dorsal and lateral). Illustrated are neurocrania in oblique frontal view with brick stresses superimposed. Warmer colors indicate higher stresses. Note the concentration of high brick stresses in the inter-orbital septum in *H. hassi* under dorsal loading compared to *P. boro*. Given that these models were given identical loading conditions (i.e. the same force per unit surface area), the neurocranium in *P. boro* is structurally stronger and better suited for head-first burrowing.

A

5mm

B

5mm

Herrel et al., Fig 4

H. hassi

P. boro

dorsal loading

lateral loading
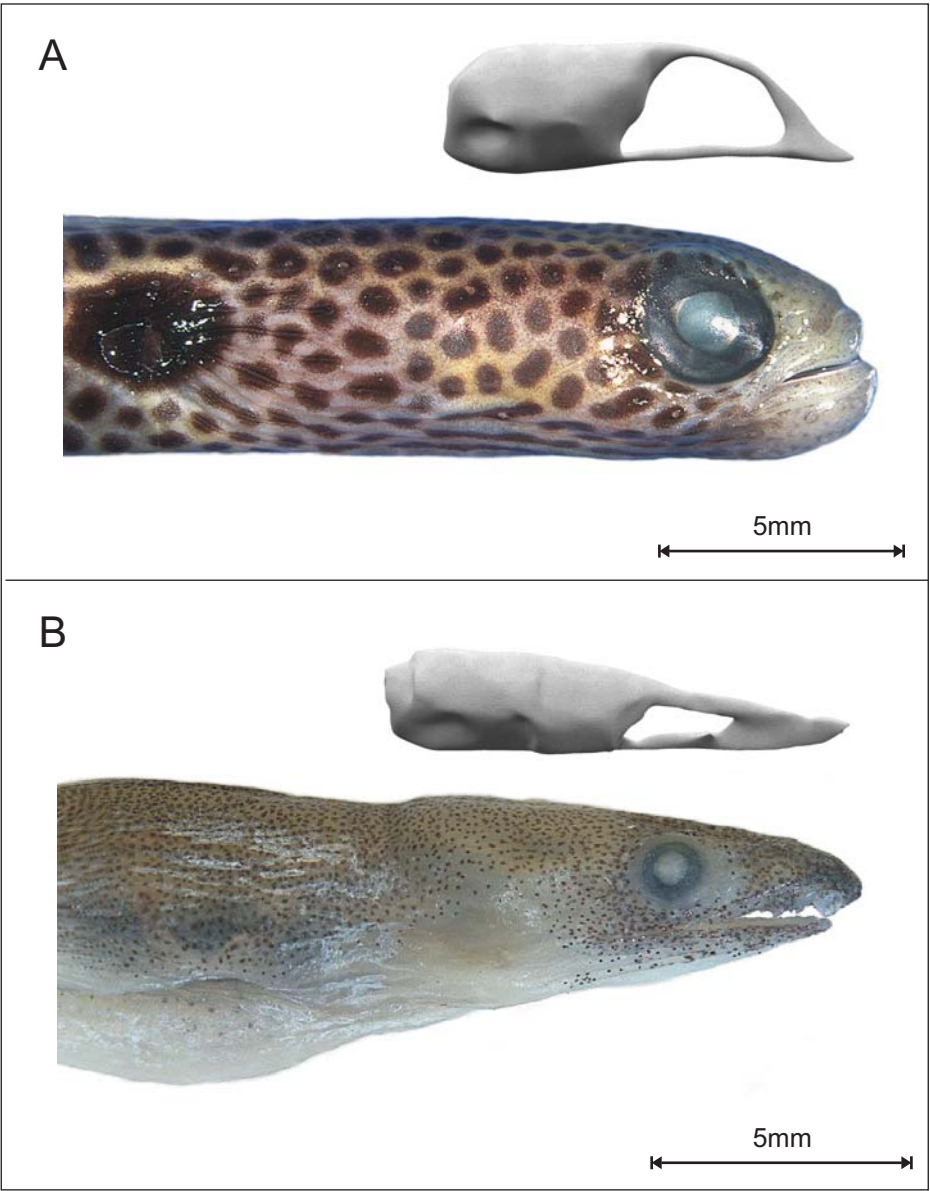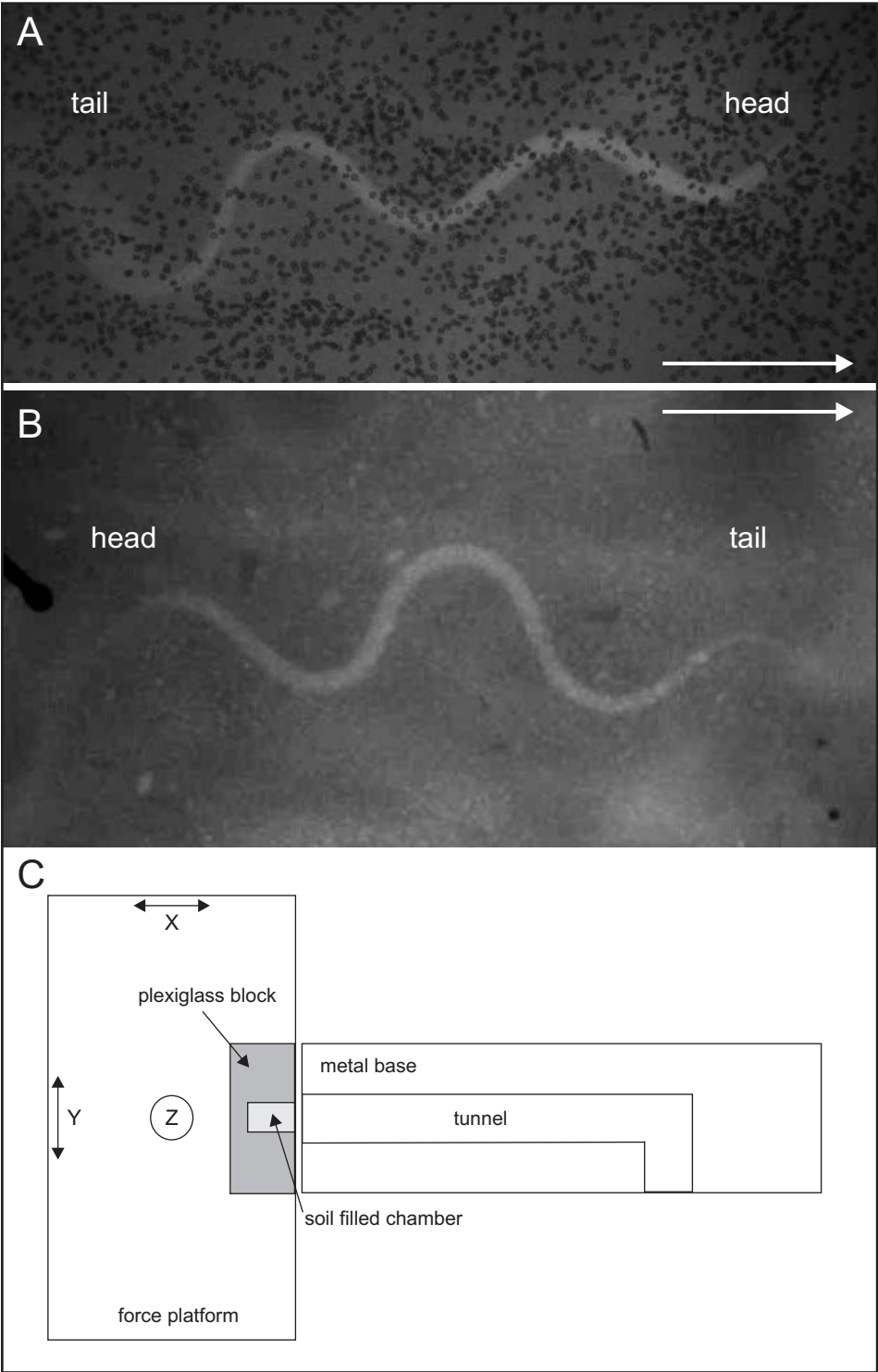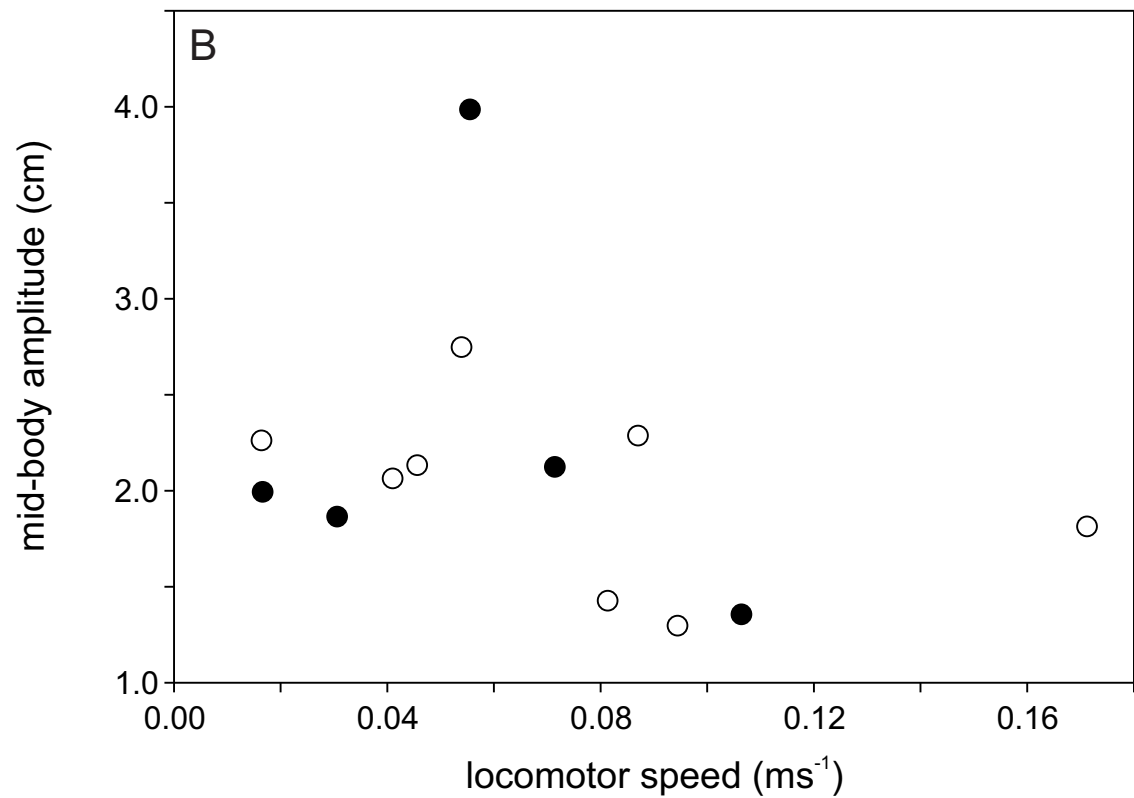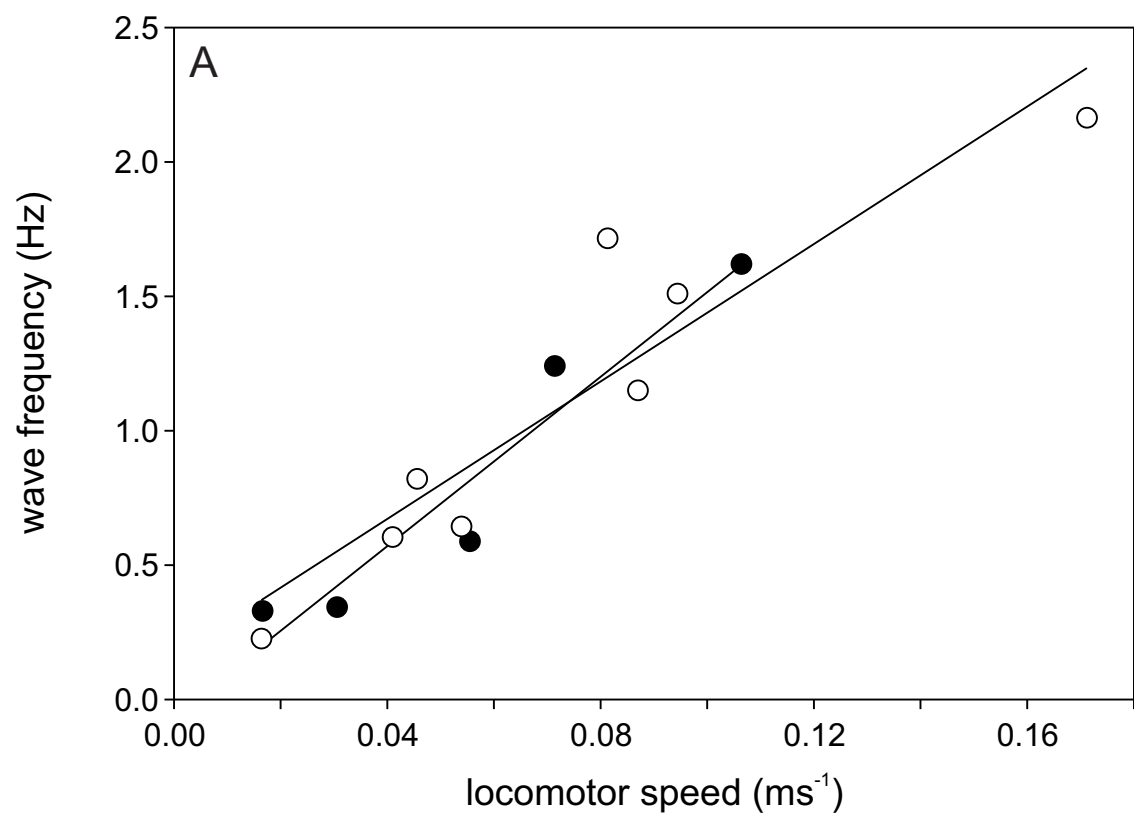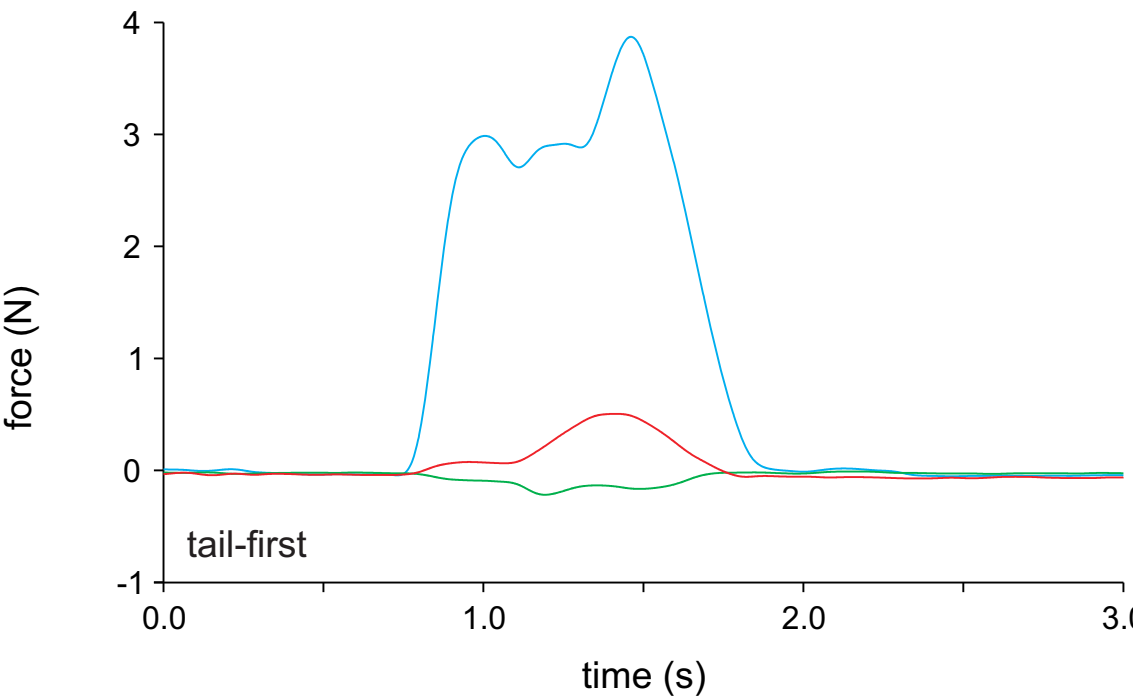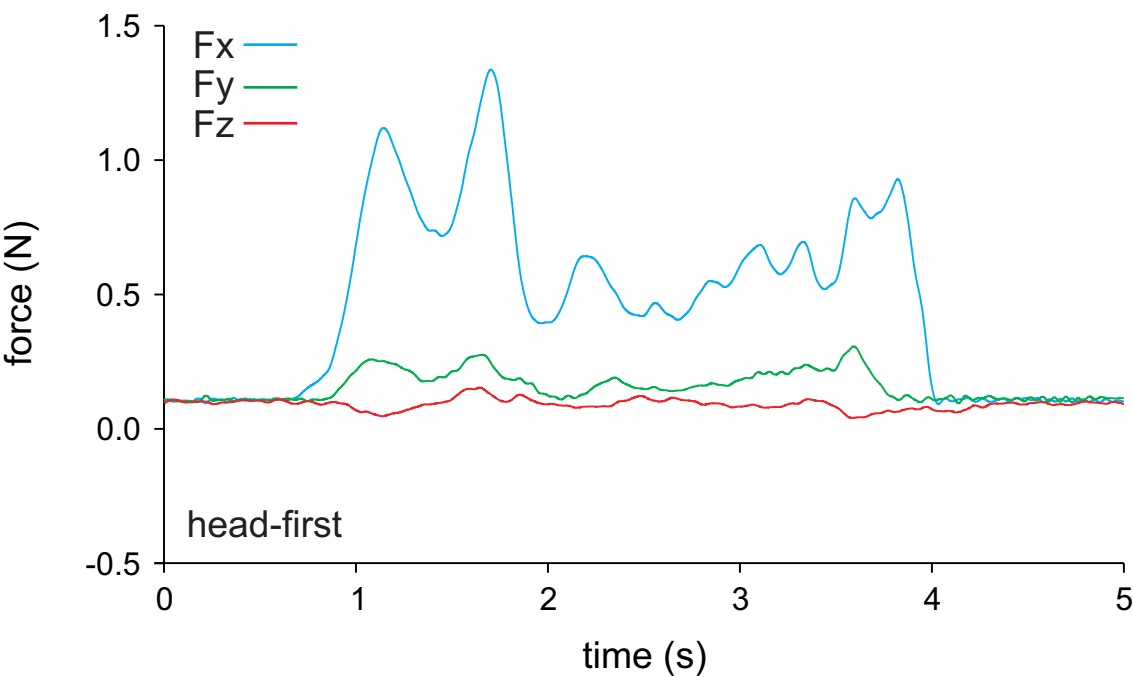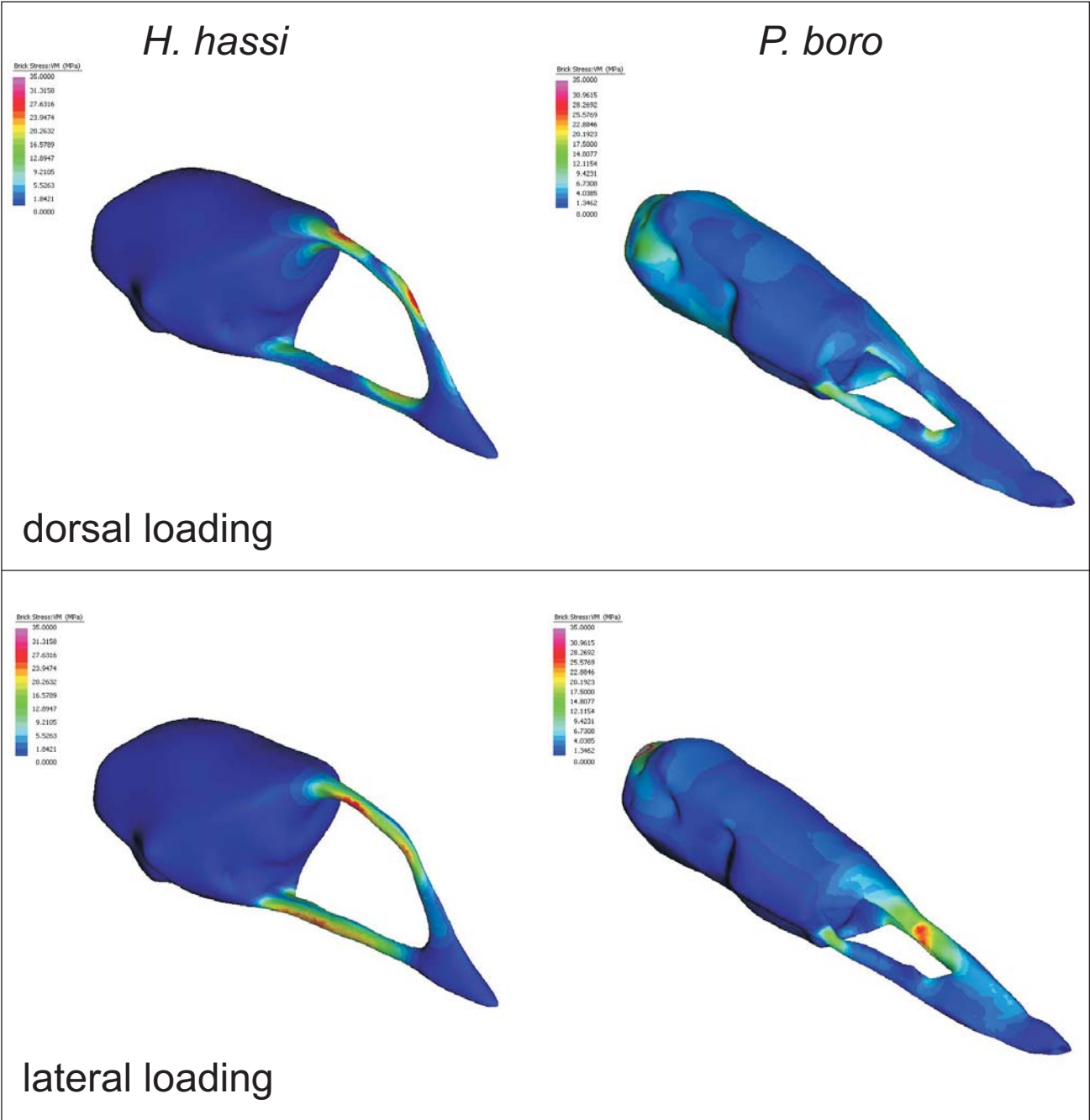
Table 1: kinematic characterization of burrowing movements in *P. boro*.

	forward (*N* = 5)	backward (*N* =8)
tail tip undulation (m)	0.011 ± 0.0035	0.012 ± 0.0029
wave frequency (Hz)	0.81 ± 0.55	1.12 ± 0.72
wave length (m)	0.067 ± 0.012	0.071 ± 0.011
wave velocity (ms-1)	0.053 ± 0.03	0.080 ± 0.057
stride length (m)	0.071 ± 0.020	0.074 ± 0.0064
amplitude COM (m)	0.0016 ± 0.0004	0.0023 ± 0.0014
slip factor	1.06 ± 0.23	1.05 ± 0.13

COM = center of mass; *N* = number of cycles analyzed.